2026 IEEE International Conference on Robotics and Automation (ICRA 2026)
June 1-5, 2026. Vienna, Austria

Shape Sensing and Tip Tracking via Reciprocating Magnet in the Soft Continuum Robot

Pingyu Xiang*, Zexi Zhao*, Hongye Zhang, Yue Wang, Rong Xiong, Haojian Lu†

***Abstract*— Soft continuum robots, attributable to inherently compliant trunks and shape manipulability, have been widely deployed in complex scenarios requiring safe human-robot interaction. However, their nonlinear deformations and hyper-redundant degrees of freedom pose substantial challenges for full-body shape sensing and closed-loop control of the end effector. A low-cost yet accurate feedback solution is thus highly desirable. To address this, we present a hydraulic-driven reciprocating magnet strategy, integrated with magnetic localization, to enable both shape sensing and tip pose estimation of soft continuum robots, thereby facilitating precise closed-loop control. The proposed approach time-multiplexes a single magnet under different operational phases to fulfill two functions: full-body shape reconstruction and tip pose tracking. We validate the effectiveness of the reciprocating magnet system on a pneumatic manipulator prototype with two active degrees of freedom. Experimental results show that the magnet can travel through the guide channel at a maximum speed of 6.5 cm/s, achieving average errors of less than 2 mm in position (1.1% of the robot's length), 3° in orientation for shape sensing and tip pose estimation. Using this sensing strategy, we demonstrate a simple closed-loop control on the soft continuum robot. Owing to its simplicity, low cost, and high precision, the proposed method holds promise as a practical alternative for state feedback in soft continuum robots.**

I. Introduction

Inspired by biological structures such as elephant trunks and octopus tentacles, soft continuum robots have been developed to operate in unstructured environments that are inaccessible to conventional rigid manipulators [1]. Owing to their intrinsic compliance, shape manipulability, and strong adaptability, they can function safely in confined, tortuous, and dynamic environments. Consequently, soft continuum robots are playing an increasingly vital role in fields such as minimally invasive surgery (MIS) [2], industrial inspection [3] and agricultural harvesting [4]. To achieve precise and reliable motion control, real-time state perception of the robot is indispensable. For rigid robots, tracking the end-effector pose is generally sufficient for motion planning and trajectory control. In contrast, the inherent deformability of soft continuum robots, together with the physical interactions arising from contact with the environment [5], renders both the robot's overall shape and its end-effector pose critical components of the state space, which directly determine the robot's manipulability.

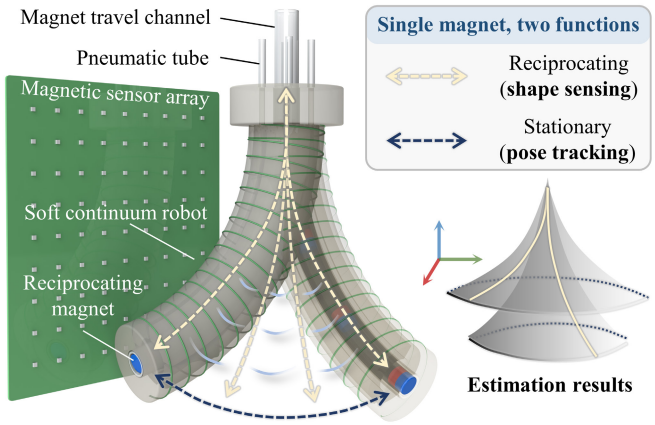

Fig. 1. Schematic illustration of shape sensing and tip tracking of a soft continuum robot using a single reciprocating magnet.

Leveraging a variety of sensing strategies and modeling approaches, numerous studies have been conducted on shape sensing and tip tracking of soft continuum robots, each achieving satisfactory results within their respective application domains. Similar to rigid manipulators, early efforts primarily relied on model-based methods, where the robot's state is inferred through kinematic and mechanical formulations. Simple kinematic models, such as the piecewise constant curvature (PCC) model [6], allow for rapid computation of robot shapes approximated by circular arcs from the actuation space. However, such oversimplified assumptions inevitably compromise accuracy and fail to capture complex scenarios involving environmental contacts. A major advancement came with the incorporation of forces into state estimation, in which the deformation of soft continua is modeled using Euler-Bernoulli beam theory [7] or Cosserat rod models [8]. These models take both actuation forces and external contact forces as inputs and have demonstrated excellent performance in shape estimation for relatively simple, homogeneous continuum robots. Nevertheless, acquiring real-time measurements of all external contact forces remains a substantial challenge.

However, due to factors such as material nonlinear elasticity, friction, and assembly imperfections, the deformation of

*These authors contribute equally. †Corresponding author.

This work was partly supported by the the National Key R&D Program of China (2025YFE0113300), National Natural Science Foundation of China (62303407, T2293720/T2293724), the State Key Laboratory of Industrial Control Technology (ICT2025A08), and Xiaomi Foundation.

Pingyu Xiang, Zexi Zhao, Hongye Zhang, Yue Wang, Rong Xiong, Haojian Lu (corresponding author) are with State Key Laboratory of Industrial Control and Technology, and Institute of Cyber-Systems and Control, Zhejiang University, Hangzhou 310027, China (email: luhaojian@zju.edu.cn).

Haojian Lu is also with the Stomatology Hospital, School of Stomatology, Zhejiang University School of Medicine, Zhejiang Provincial Clinical Research Center for Oral Diseases, Zhejiang Key Laboratory of Oral Biomedical, Engineering Research Center of Oral Biomaterials and Devices of Zhejiang Province, Hangzhou, China.

soft continuum robots induced by actuation and interactions with the environment is highly complex in practice. This complexity poses significant limitations for describing their states solely through kinematic or dynamic models. With the rapid advancement of artificial intelligence, a growing number of learning-based approaches for shape sensing have emerged. For example, Shentu *et al*. proposed MoSSNet, a deep encoder-decoder network capable of inferring the contour of a continuum robot from a single monocular camera [9]. Similarly, Ha *et al*. employed artificial neural networks (ANNs) to directly learn the robot's shape [10]. While learning-based methods show promising performance, they often require extensive data collection and careful network design during the training phase, and their generalization capability across different robots and scenarios remains an important consideration.

Beyond model-based approaches, directly acquiring the robot's shape through various external or embedded sensors has emerged as a promising direction. External sensing relies on devices that capture shape information from outside the robot, such as visual imaging or electromagnetic tracking. In MIS, for instance, surgeons often prefer to obtain the shape of continuum guidewires intraoperatively via real-time digital subtraction angiography (DSA) to ensure safe navigation [11]. Croom *et al*. employed self-organizing maps to extract the robot's backbone curve from depth-camera point clouds [12]. Internal sensing, in contrast, integrates sensors within the robot itself to directly measure deformations, making it less susceptible to line-of-sight occlusions. For example, in continuum robots larger than guidewires, fiber Bragg grating (FBG) sensors that are renowned for their high accuracy and long-term stability have been adopted in applications such as bronchoscopy robots for shape reconstruction [13]. However, their brittleness and the high cost of demodulation units have hindered widespread adoption in low-cost soft continuum robots. Alternatively, flexible resistive, piezoresistive, and capacitive sensors [14], [15] have been designed to measure deformations. These approaches are inherently well-suited to the compliant nature of soft continuum robots, though ensuring consistency and reliability remains a challenge.

Tip tracking can be realized in a more straightforward manner, for instance by directly mounting sensors at the robot's tip. In principle, achieving full-shape reconstruction is equivalent to obtaining tip tracking. however, for reconstruction methods prone to cumulative errors, tip tracking is often not their strength. For example, FBG sensors estimate shape through strain integration, which leads to the largest uncertainty accumulating at the distal end. In addition, most learning-based reconstruction methods optimize their objective functions with respect to global shape accuracy rather than tip accuracy, which may fall short of the stringent requirements for high-precision tip tracking.

The brief survey of existing shape estimation approaches for soft continuum robots reveals a clear unmet need: the development of low-cost, user-friendly, and accurate shape estimation methods, ideally with the ability to directly track tip pose for precise closed-loop control. Magnetic-based techniques have emerged as a promising avenue to address these challenges. As a low-cost and non-contact sensing modality, they are capable of operating under line-of-sight occlusions [16]. Researchers have explored various strategies for magnetic shape sensing of soft continuum robots. For example, Wang *et al*. localized two embedded magnets using a sensor array and fitted the robot's shape with a Bézier curve [17]. Guo *et al*. sequentially arranged magnetometers and magnets along the robot trunk, computing angular variations between successive pairs to reconstruct a piecewise circular-arc shape [18]. Pittiglio *et al*. designed a chain of magnetic balls inserted inside the central lumen of the robot, where bending-induced field variations were used to fit the robot shape with a single circular arc [19]. While these studies successfully leveraged magnetic fields for shape sensing, their reliance on simplified assumptions, such as circular-arc or Bézier representations, remains a limitation. Because the sensing units are discretely distributed along the trunk, the resulting measurements cannot provide continuous and precise position and orientation information along the backbone, particularly at the robot's distal tip.

Motivated by the aforementioned studies, this work aims to propose an alternative approach to address their limitations. Specifically, we introduce a method that reconstructs the shape of a soft continuum robot by hydraulically driving a magnet to reciprocally scan along the robot's trunk, with its pose continuously tracked via magnetic localization, as illustrated in Fig. 1. Unlike prior methods, our approach requires only a single magnet, which is time-multiplexed to simultaneously achieve both shape reconstruction and tip pose tracking. Notably, since the magnet theoretically traverses all positions along the robot's trunk during its motion, this sensing strategy is capable of providing continuous position and orientation information along the backbone an ability that has not been realized in previous magnetic-based shape sensing techniques.

The remainder of this paper is organized as follows. Section II introduces the magnetic localization method based on the sensor array employed in this study. Section III details the system design of the pneumatic continuum robot equipped with the reciprocating magnet device. Section IV presents characterization experiments, including both shape sensing and closed-loop tip tracking control. Finally, Section V concludes the paper.

II. Methodology

A. Problem Formulation

We achieve both shape estimation and tip pose tracking of a soft continuum robot of length L by exploiting a magnet that reciprocates within the robot body. The key to this task lies in the real-time localization of the internal magnet using an external array of magnetic sensors, as illustrated in Fig. 2. In this work, the relative pose between two coordinate frames is described by a displacement vector ${}^{a}\boldsymbol{u}_{b} \in \mathbb{R}^{3}$ and an orientation vector ${}^{a}\boldsymbol{\theta}_{b} \in \mathfrak{se}(3)$, where the indices a and b denote the reference and the current coordinate

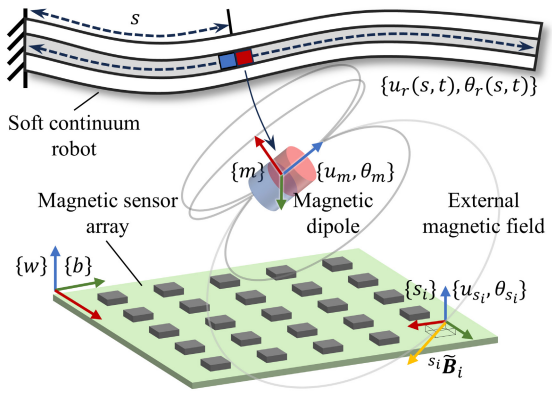

Fig. 2. Illustration of magnetic dipole localization with an external magnetic sensor array.

frames, respectively. The exponential map $\mathrm{Exp}(\cdot)$ is used to transform from $\mathfrak{so}(3)$ to $SO(3)$.

Formally, four coordinate frames are involved in this problem: the world frame $\{w\}$, the PCB board frame $\{b\}$, the local frames of the N sensors $\{s_i\}$, and the frame attached to the magnet $\{m\}$. Without loss of generality, we assume that the world frame $\{w\}$ coincides with the board frame $\{b\}$, thereby simplifying the problem formulation. According to the PCB design, the poses of all sensor frames $\{s_i\}$ are known and are uniquely determined with respect to $\{w\}(\{b\})$. The robot's motion state is represented as ${}^{w}\boldsymbol{u}_r(s,t)$ and ${}^{w}\boldsymbol{\theta}_r(s,t)$, where $s \in [0, L]$ denotes the arc length along the body and t denotes time. It is worth noting that the magnet employed in this work is a cylindrical permanent magnet, a widely used configuration in the literature. The degree of freedom corresponding to rotation about its intrinsic z-axis is unobservable; however, this limitation does not affect its applicability in geometrically symmetric continuum robots.

The measurement of the i-th sensor is denoted as ${}^{a}\tilde{\boldsymbol{B}}_i$. Since the magnetic field is a three-dimensional vector, the reference coordinate frame $\{a\}$ of each measurement must be specified. In the following, we assume that all sensor readings have been pre-processed by subtracting the background magnetic field and intrinsic sensor bias measured in the absence of the magnet.

For notational simplicity, the world frame $\{w\}$ is omitted in the subsequent formulations.Therefore, the problem can be formulated as follows: given the known poses of the sensor array $\{\boldsymbol{u}_{s_i}, \boldsymbol{\theta}_{s_i}\}$ and the measured magnetic fields ${}^{a}\tilde{\boldsymbol{B}}_i$, infer the pose of the magnet $\{\boldsymbol{u}_m, \boldsymbol{\theta}_m\}$ at time t, and subsequently reconstruct the robot's shape $\{\boldsymbol{u}_r(s,t), \boldsymbol{\theta}_r(s,t)\}$ or track the tip pose $\{\boldsymbol{u}_r(L,t), \boldsymbol{\theta}_r(L,t)\}$.

B. Magnetic Localization

We model the magnet in the soft continuum robot as a magnetic dipole, which is a widely adopted approximation [20]. In its own coordinate frame $\{m\}$, the external magnetic field generated by this dipole at a point $\boldsymbol{p} \in \mathbb{R}^3$ can be expressed as,

$$\boldsymbol{\mathcal{B}}(\boldsymbol{p}) = \frac{\mu_0}{4\pi}\left(\frac{3(\boldsymbol{m}\cdot\boldsymbol{p})\boldsymbol{p}}{||\boldsymbol{p}||^5} - \frac{\boldsymbol{m}}{||\boldsymbol{p}||^3}\right), \tag{1}$$

where μ_0 is the permeability of the free space and $\boldsymbol{m} = [0, 0, \mathrm{m}]^T$ denotes the magnetic dipole moment vector.

For the i-th sensor, after transforming the magnetic field into the local sensor frame, the theoretical magnetic flux density can be obtained according to the dipole field model as follows:

$${}^{s_i}\boldsymbol{B}_i = \mathrm{Exp}(-\boldsymbol{\theta}_{s_i})\mathrm{Exp}(\boldsymbol{\theta}_m)\cdot\boldsymbol{\mathcal{B}}(\mathrm{Exp}(-\boldsymbol{\theta}_m)(\boldsymbol{u}_{s_i} - \boldsymbol{u}_m)). \tag{2}$$

Magnetic localization is thus formulated as a nonlinear optimization problem, where the measurements from multiple sensors are combined and the optimization variables are the position $\boldsymbol{u}_m$ and orientation $\boldsymbol{\theta}_m$ of the magnet. The objective function is defined as,

$$f(\boldsymbol{u}_m, \boldsymbol{\theta}_m) = \sum_{i=1}^{N} ||\,{}^{s_i}\boldsymbol{B}_i - {}^{s_i}\tilde{\boldsymbol{B}}_i||^2. \tag{3}$$

By minimizing Eq. (3), the estimated pose of the magnet is obtained. To handle the inherent nonlinearity, we further derive the partial derivatives of the magnetic field model with respect to both the magnet's position and orientation. Using the chain rule, these derivatives enable straightforward computation of the Jacobian matrix of the objective function with respect to the optimization variables, which significantly accelerates convergence and enhances the real-time performance of magnetic localization.

Taking the derivative of Eq. (1) with respect to $\boldsymbol{p}$, we obtain the magnetic field gradient tensor as follows,

$$\begin{aligned}\boldsymbol{\mathcal{H}}(\boldsymbol{p}) = \nabla\boldsymbol{\mathcal{B}}(\boldsymbol{p}) = \frac{3\mu_0}{4\pi||\boldsymbol{p}||^7}\cdot \\ \left(||\boldsymbol{p}||^2\left(\boldsymbol{p}\boldsymbol{m}^T + \boldsymbol{m}\boldsymbol{p}^T + (\boldsymbol{m}^T\boldsymbol{p})\mathbf{I}_3\right) - 5\boldsymbol{m}^T\boldsymbol{p}(\boldsymbol{p}\boldsymbol{p}^T)\right)\end{aligned} \tag{4}$$

Subsequently, differentiating the measurement function with respect to the magnet position $\boldsymbol{u}_m$ yields:

$$\begin{aligned}\boldsymbol{J}^i_{\boldsymbol{u}_m} &= \frac{\partial\,{}^{s_i}\boldsymbol{B}_i}{\partial\boldsymbol{u}_m} \\ &= \frac{\partial\mathrm{Exp}(-\boldsymbol{\theta}_{s_i})\mathrm{Exp}(\boldsymbol{\theta}_m)\cdot\boldsymbol{\mathcal{B}}(\boldsymbol{p}_i)}{\partial\boldsymbol{p}_i}\cdot\frac{\partial\boldsymbol{p}_i}{\partial\boldsymbol{u}_m} \\ &= \mathrm{Exp}(-\boldsymbol{\theta}_{s_i})\mathrm{Exp}(\boldsymbol{\theta}_m)\cdot\boldsymbol{\mathcal{H}}(\boldsymbol{p}_i)\cdot(-\mathrm{Exp}(-\boldsymbol{\theta}_m)),\end{aligned} \tag{5}$$

and with respect to the magnet orientation $\boldsymbol{\theta}_m$ gives:

$$\begin{aligned}\boldsymbol{J}^i_{\boldsymbol{\theta}_m} =& \frac{\partial\,{}^{s_i}\boldsymbol{B}_i}{\partial\boldsymbol{\theta}_m} \\ =& -\mathrm{Exp}(-\boldsymbol{\theta}_{s_i})(\mathrm{Exp}(\boldsymbol{\theta}_m)\boldsymbol{\mathcal{B}}(\boldsymbol{p}_i))^\wedge\cdot\boldsymbol{J}_l(\boldsymbol{\theta}_m) \\ &+ \mathrm{Exp}(-\boldsymbol{\theta}_{s_i})\mathrm{Exp}(\boldsymbol{\theta}_m)\cdot\boldsymbol{\mathcal{H}}(\boldsymbol{p}_i)\cdot(\boldsymbol{p}_i)^\wedge\cdot\boldsymbol{J}_l(-\boldsymbol{\theta}_m),\end{aligned} \tag{6}$$

where $\boldsymbol{p}_i = \mathrm{Exp}(-\boldsymbol{\theta}_m)(\boldsymbol{u}_{s_i} - \boldsymbol{u}_m)$, $\boldsymbol{J}_l(\cdot)$ denotes the left Jacobian of the exponential map used for linearization [21], and the $(\cdot)^\wedge$ operator represents the skew-symmetric matrix associated with a 3-vector.

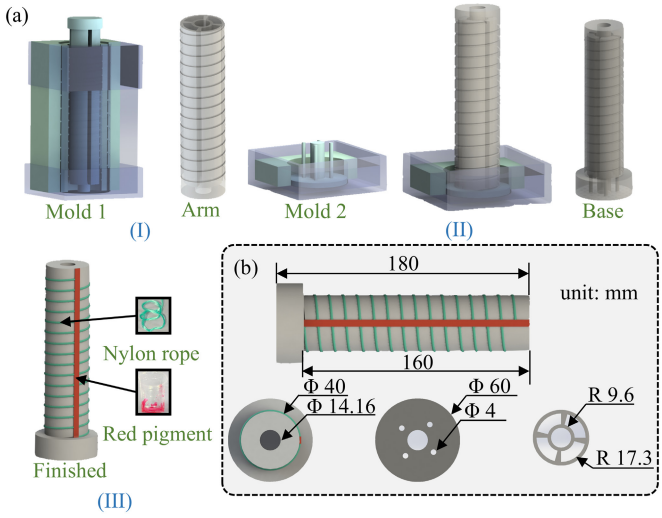

Fig. 3. Illustration of a continuum robot.(a) Detailed fabrication process. (b) Geometric dimensions of the robot.

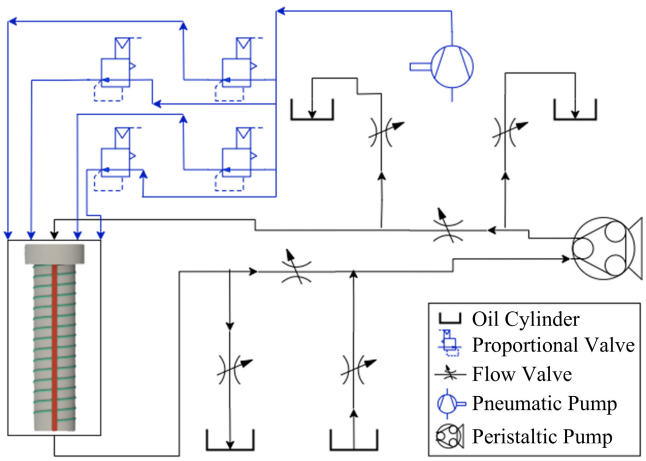

Fig. 4. Schematic diagram of the actuation system of the pneumatic soft continuum robot and the hydraulic system driving the reciprocating motion of the magnet.

To solve this nonlinear least-squares problem, we employ the Levenberg-Marquardt (LM) algorithm, which combines the advantages of Gauss-Newton and gradient descent. Moreover, we explicitly provide the analytical gradients in the implementation to improve optimization efficiency.

III. System Design

A. Pneumatic Soft Continuum Robot

The fabrication process of the pneumatic soft continuum robot, featuring a central hydraulic channel, consists of three main steps, as illustrated in Fig. 3, and is detailed as follows:

1) Arm: The silicone mixture for the manipulator's main body is prepared. 75 g of Dragon Skin™ 20 Part A and 75 g of Part B (1:1 by weight) are thoroughly mixed with 2.4 g of white silicone pigment (1.6% of the total silicone weight). The mixture is then initially degassed in a vacuum chamber. To prevent the reintroduction of air bubbles during pouring, the central core of Mold 1 is temporarily removed before the silicone is poured into the mold's outer shell. Subsequently, the core is carefully reinserted from above into the silicone-filled mold. The entire assembly is then placed back into the vacuum chamber for a final degassing step to eliminate any remaining air bubbles. After curing at room temperature for 4 hours, the molded continuum arm is demolded (Fig. 3(a)(I)).

2) Base: The continuum arm is then placed into Mold 2. Subsequently, the silicone mixture for the base is prepared: 15 g of Dragon Skin™ 20 Part A, 15 g of Part B, and 0.48 g of white pigment are mixed and degassed. This mixture is then poured into the base cavity of Mold 2. The silicone solidifies at the bottom of the mold, forming the robot's base and fusing with the pre-placed arm. After curing at room temperature for 4 hours, the molded continuum base is demolded (Fig. 3(a)(II)).

3) Finished: A nylon rope is precisely wound into the helical grooves on the manipulator's surface to act as a strain-limiting layer. This reinforcement prevents lateral deformation (i.e., radial expansion) and ensures the robot maintains a constant diameter during actuation. A small amount of freshly prepared Dragon Skin™ 20 mixture is applied as an adhesive to secure the rope in place. After curing for 4 hours, the rope is firmly integrated with the robot arm. This completes the fabrication of the continuum robot (Fig. 3(a)(III)). The geometric dimensions of each component of the robot are illustrated in Fig. 3(b).

B. Pneumatic and Hydraulic Actuation System

As illustrated by the blue pipelines in Fig. 4, the actuation system of the pneumatic soft continuum robot primarily consists of an air pump and four proportional valves, each precisely regulating the pressure of a corresponding chamber. By dynamically adjusting the inlet airflow, the chamber pressures can be modulated, thereby enabling continuous control of the robot's motion state.

To enable shape sensing via a mobile internal magnetic source, we designed a hydraulic system that precisely controls the reciprocating motion of a permanent magnet. The system's architecture, represented by the black pipelines in Fig. 4, illustrates its working principle.

The core of the hydraulic system is a peristaltic pump, which propels a permanent magnet within the robot's central channel (7 mm ID). The pump's speed and direction are precisely managed, enabling controlled motion. During the initial setup, the circuit is primed by operating the pump in conjunction with six manually adjusted flow valves to completely fill the pipeline with methyl silicone oil. Afterward, the system is sealed to create a closed-loop configuration for bi-directional actuation.

The selection of methyl silicone oil as the hydraulic medium is critical. Its high viscosity provides stable and smooth propulsion, while its lubricating properties guarantee low-friction movement in the confined space. Together, these

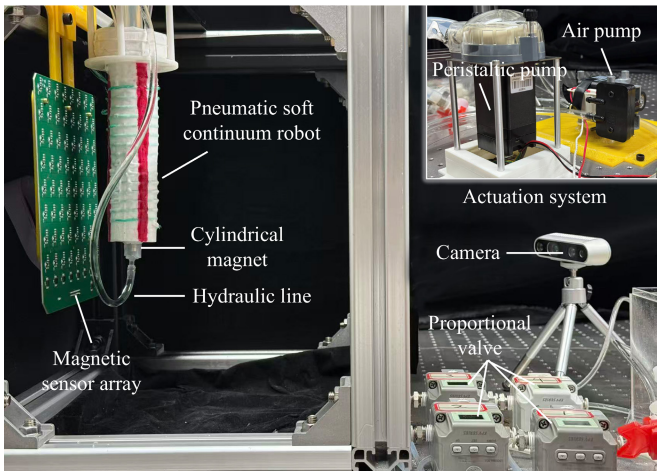

Fig. 5. Experimental Setup. The proposed pneumatic soft continuum robot with a hydraulic reciprocating magnet primarily consists of a magnetic sensor array, the robot body, a proportional valve for precise pressure control, and an actuation system composed of an air pump and a peristaltic pump.

characteristics ensure the reliability and feasibility of this shape sensing approach.

IV. Experimental Results

A. Experimental Setup

The main components of the system are shown in Fig. 5. An 8 × 8 array of LIS2MDL (STMicroelectronics) three-axis magnetometers forms the magnetic sensor array, which is mounted on the back of the soft continuum robot. A cylindrical magnet (Ø6 mm × 10 mm) is smoothly actuated within a silicone tube of 7 mm inner diameter embedded in the robot's body, driven by an LFP404ST (LEFOO) peristaltic pump. Robot actuation is achieved pneumatically. An air pump supplies air to four independent chambers, each governed by an EPV1-30MD2 proportional valve. These valves modulate the pressure in each chamber to control the robot's multi-directional bending postures.

B. Motion of the Magnet

To evaluate the motion behavior of the magnet within the conduit, we analyzed its velocity as a function of leaning angle at a constant pump speed.

The magnet was actuated in a straight tube at various leaning angles from 0° (vertical) to 90° (horizontal) as shown in Fig. 6(a). The results in Fig. 6(b) show that the inclination angle significantly impacts the speed difference between upward and downward travel. As the tube approaches a horizontal orientation (90°), the effect of gravity is minimized, and the two speeds converge. Conversely, the speed difference is maximized at the vertical orientation (0°). This state-dependent velocity is crucial for evaluation of the refresh rate of shape sensing.

C. Shape Sensing

We first evaluated the performance of the proposed magnetic localization system, as shown in Fig. 7(a). At three

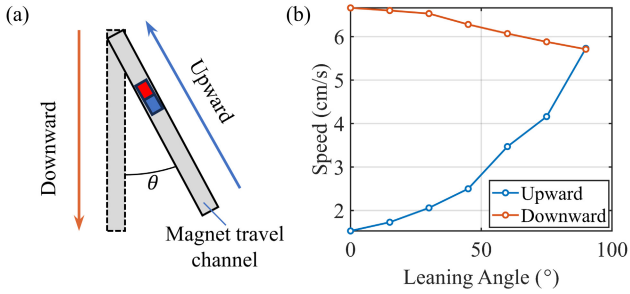

Fig. 6. Magnet translation speed in conduits with different orientations. (a) Schematic diagram. (b) linear motion speed of the magnet with respect to the leaning angle.

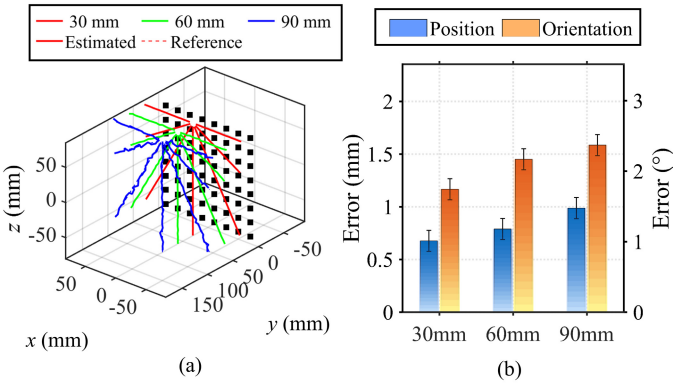

Fig. 7. Magnetic localization along straight trajectories at different distances. (a) localization results for straight trajectories at 30 mm, 60 mm, and 90 mm from the sensor array; (b) position and orientation errors at the three distances.

representative working distances of the robot (30 mm, 60 mm and 90 mm), we designed magnet trajectories that commonly arise in the shape sensing scenario of this robot, extending outward from the central top of the sensor array. The magnet was moved along these trajectories, and its pose was estimated using the optimized algorithm described in Section II. Leveraging the analytical form of the Jacobian matrix, the computation time for each pose estimation, with 64 sensor observations, was less than 25 ms on a standard laptop computer (CPU: AMD Ryzen 7 7840H), which is sufficient to meet the real-time requirements of state feedback and closed-loop control. The localization errors at the three distances are shown in Fig. 7(b). Although the errors increase with distance, as expected, the system consistently maintains high accuracy across a considerable workspace (greater than 12 cm). The position and orientation errors remain below 2 mm and 3°, respectively, demonstrating that magnetic localization can serve as a reliable state-sensing approach for soft continuum robots with centimeter-scale diameters.

Furthermore, to demonstrate the capability of the proposed magnetic localization system for shape sensing within the actual robot, we evaluated its performance under two different bending magnitudes. For each bending condition, the robot was bent around its vertical axis at intervals

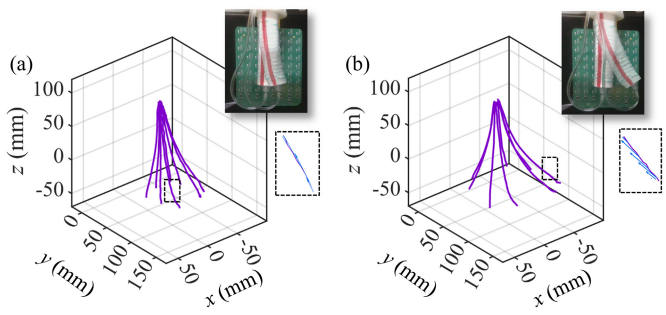

Fig. 8. Shape sensing results using the proposed system. (a) Robot shape under a small bending angle. (b) Robot shape under a large bending angle.

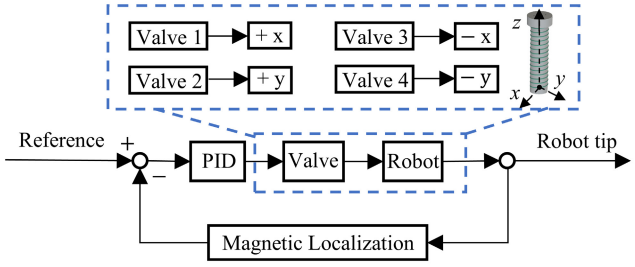

Fig. 9. Block diagram of the closed-loop PID control for the robot's tip. The tip position is measured by the magnetic localization system and compared to a reference trajectory. The resulting error signal is fed to a PID controller, which modulates the four pneumatic valves to actuate the robot.

of 45° in different orientations. The corresponding results are presented in Fig. 8. It should be noted that the robot was still operated in an open-loop control mode, and thus the bending amplitudes were not exactly identical across orientations. The results confirm that, within the real robotic system, the reciprocating magnet can indeed reconstruct the robot's continuous shape with high fidelity. Importantly, beyond recovering positional information of the shape, the cylindrical magnet's orientation is constrained by the internal fluidic conduit, enabling estimation of the local orientation of the robot's trunk axis, as highlighted in the magnified view of Fig. 8.

D. Tip Pose Tracking

Beyond full-body shape sensing, our system's dual-mode capability allows for high-precision, closed-loop control of the robot's tip. For this control task, the hydraulic system pushes the magnet to the distal end of the robot's central channel, where it remains stationary. The magnetic localization system then provides continuous, real-time measurements of the magnet's pose, which directly corresponds to the robot's tip pose.

We implemented a closed-loop control system, as illustrated in Fig. 9. A Proportional-Integral-Derivative (PID) controller was designed to minimize the error between a desired reference trajectory and the real-time tip position measured by the magnetic localization system. The controller's output adjusts the duty cycle of the four proportional valves, thereby modulating the pressure in the corresponding pneumatic chambers to steer the robot's tip accurately. It is worth noting that the continuum robot used for method validation in this study possesses only two active degrees of freedom. Consequently, the closed-loop control considers solely the position feedback in the $x - y$ plane.

To emphasize the aspect of closed-loop control enabled by the proposed method, we tasked the robot with tracking two distinct trajectories: a cross pattern and three concentric squares of varying sizes. For comparison, we conducted both open-loop and closed-loop trials for each trajectory. In the open-loop trials, the robot was driven by a predetermined sequence of pressure commands without any feedback. As shown in Fig. 10(a) and (c), the resulting paths exhibit significant deviations, overshoot, and shape distortion

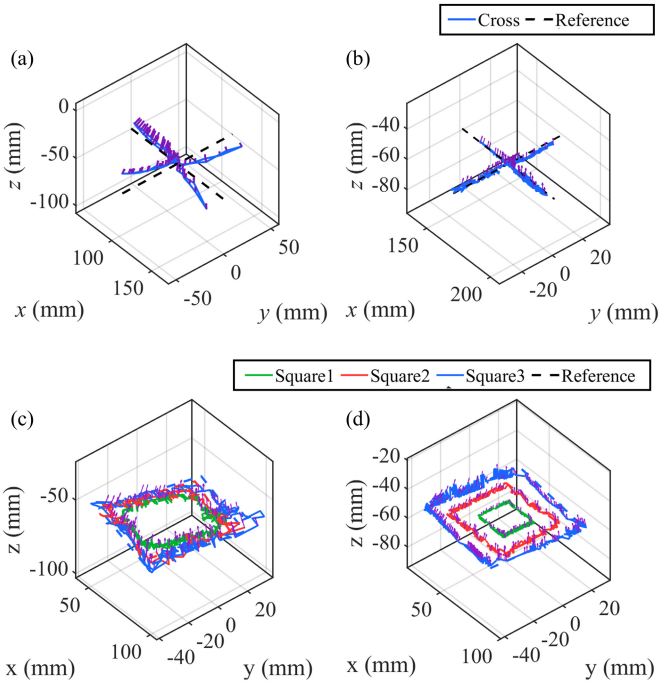

Fig. 10. Experimental results comparing open-loop and closed-loop tip trajectory tracking. (a) Open-loop and (b) closed-loop control for a cross-shaped path. (c) Open-loop and (d) closed-loop control for three concentric square-shaped paths.

compared to the reference trajectories (dashed black lines). These inaccuracies are attributable to the inherent hysteresis and nonlinear dynamics of the soft pneumatic actuator.

In contrast, enabling closed-loop control with magnetic feedback markedly enhanced the tracking performance. As shown in Fig. 10(b) and (d), the robot tip closely followed the reference cross and square trajectories with high fidelity. With position feedback provided by the magnetic localization system, the chamber pressures were effectively regulated (Fig. 11), allowing the robot to accurately track the target paths with an error less than 2 mm. The controller successfully compensated for system nonlinearities, yielding precise and stable motion. These results demonstrate that the proposed magnetic localization approach provides a reliable and accurate feedback source for the real-time control of soft continuum robots.

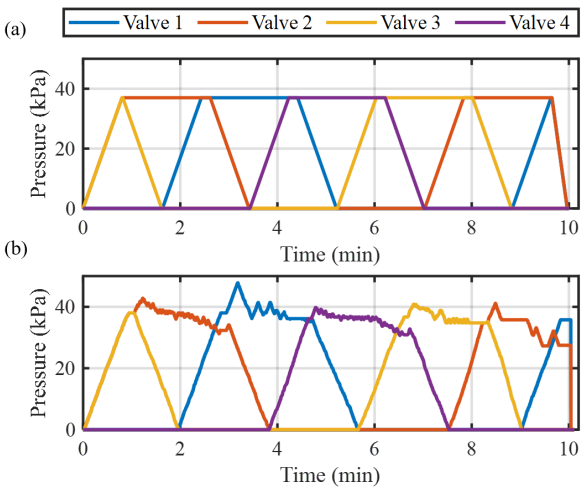

Fig. 11. Pressure variations in the four chambers under open-loop and closed-loop control. (a) Open-loop control, (b) Closed-loop control.

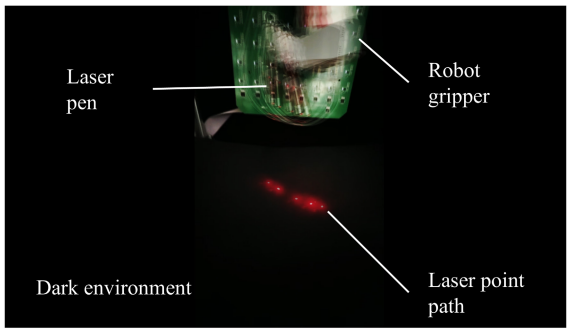

Fig. 12. Experimental setup for operating the soft continuum robot in a dark, vision-constrained environment.

E. Dual Sensing-Mode Operation

Shape sensing and precise tip control are critical for soft continuum robots, particularly in vision-constrained environments. To emulate such conditions and demonstrate the proposed system's capability for both high-precision tip tracking and full-body shape sensing, we first placed the robot in a dark environment, simulating scenarios like industrial inspection where external visibility is limited. This setup highlights the advantage of magnetic localization sensing, which is inherently unaffected by optical occlusion. A laser pointer was mounted at the robot's tip, serving both to evaluate the tip motion and to mimic practical tasks in which the robot carries a laser or light source for exploration, measurement, or inspection guidance as shown in Fig. 12.

we then executed a relatively complex trajectory task: guiding the robot's end effector to trace the letters "Z," "J," and "U" in free space (Fig. 13). This experiment is intuitive for validating the time-multiplexed operation of the single reciprocating magnet for comprehensive state perception.

The trajectory execution was implemented using a hybrid sensing strategy that alternates between two distinct modes. The process begins with tip tracking mode: the magnet is held stationary at the robot's distal end, providing continuous

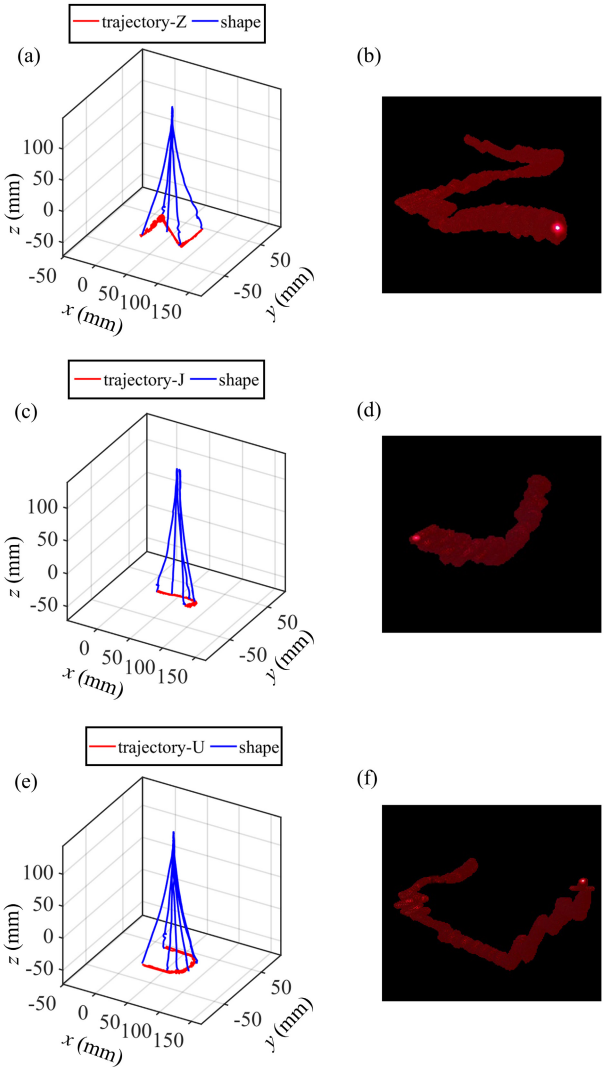

Fig. 13. Experimental validation of the proposed shape sensing and tip tracking. (a), (c), (e) Robot end-tip trajectories and reconstructed shapes for the letters "Z", "J", and "U", respectively. (b), (d), (f) Corresponding laser paths traced in a dark background.

pose feedback to the PID controller, which modulates the pneumatic actuation to follow the defined path. At some critical points along the trajectory, such as corners or transitions, the tip-tracking execution is paused. The system then switches to shape sensing mode: the hydraulic system activates the peristaltic pump, driving the magnet to reciprocate along the entire length of the robot's central lumen. During this rapid scan, the magnetic localization system acquires continuous position and orientation data along the robot, enabling the reconstruction of the robot's shape. Upon the completion of the shape scan, the magnet is returned to the tip, and the closed-loop tracking mode resumes to continue the trajectory task.

In Fig. 13, we demonstrate a dynamic, intermittent approach for shape sensing and tip tracking of the soft continuum robot. The reconstructed shapes are shown as blue curves in Fig. 13(a), (c), and (e), while the red trajectories

on the left and the laser patterns swept by the tip illustrate the tracked paths. This capability is particularly significant, as it allows the robot to monitor its configuration in real time during tip-level control. For instance, the system can identify unexpected contacts that induce abnormal body deformations, thereby enhancing safety and reliability in constrained or unstructured environments.

V. Conclusions

In this work, we presented a hydraulic-driven reciprocating magnet strategy integrated with magnetic localization to achieve both shape sensing and tip pose tracking in soft continuum robots. By time-multiplexing a single internal magnet between scanning and stationary modes, the proposed system enables continuous reconstruction of the robot's backbone and accurate estimation of the distal tip pose. Experimental validation on a pneumatic continuum robot prototype demonstrated high localization accuracy, with position and orientation errors below 2 mm and 3°, respectively, and a computational latency of only 25 ms per pose estimation. Leveraging this sensing capability, we implemented closed-loop tip trajectory control, significantly improving tracking fidelity over open-loop operation. Furthermore, dual-mode experiments under vision-constrained conditions highlighted the potential of this approach for practical applications such as industrial inspection and minimally invasive surgery.

Owing to its simplicity, low cost, and robustness to optical occlusion, the proposed method provides a promising alternative for real-time state feedback in soft continuum robots. Future work will explore scaling the approach to robots with higher degrees of freedom, extending its applicability to more complex tasks and unstructured environments, and integrating learning-based control strategies to further enhance autonomy.

References

[1] M. Russo, S. M. H. Sadati, X. Dong, A. Mohammad, I. D. Walker, C. Bergeles, K. Xu, and D. A. Axinte, "Continuum robots: An overview," *Advanced Intelligent Systems*, vol. 5, no. 5, p. 2200367, 2023.

[2] J. Burgner-Kahrs, D. C. Rucker, and H. Choset, "Continuum robots for medical applications: A survey," *IEEE transactions on robotics*, vol. 31, no. 6, pp. 1261–1280, 2015.

[3] M. Wang, X. Dong, W. Ba, A. Mohammad, D. Axinte, and A. Norton, "Design, modelling and validation of a novel extra slender continuum robot for in-situ inspection and repair in aeroengine," *Robotics and Computer-Integrated Manufacturing*, vol. 67, p. 102054, 2021.

[4] J. F. Elfferich, D. Dodou, and C. Della Santina, "Soft robotic grippers for crop handling or harvesting: A review," *Ieee Access*, vol. 10, pp. 75 428–75 443, 2022.

[5] M. B. Wooten and I. D. Walker, "Environmental interaction with continuum robots exploiting impact," *IEEE Robotics and Automation Letters*, vol. 7, no. 4, pp. 10 136–10 143, 2022.

[6] R. J. Webster III and B. A. Jones, "Design and kinematic modeling of constant curvature continuum robots: A review," *The International Journal of Robotics Research*, vol. 29, no. 13, pp. 1661–1683, 2010.

[7] G. Wu, G. Shi, and Y. Shi, "Modeling and analysis of a parallel continuum robot using artificial neural network," in *2017 IEEE International Conference on Mechatronics (ICM)*. IEEE, 2017, pp. 153–158.

[8] J. Till, V. Aloi, and C. Rucker, "Real-time dynamics of soft and continuum robots based on cosserat rod models," *The International Journal of Robotics Research*, vol. 38, no. 6, pp. 723–746, 2019.

[9] C. Shentu, E. Li, C. Chen, P. T. Dewi, D. B. Lindell, and J. Burgner-Kahrs, "Moss: Monocular shape sensing for continuum robots," *IEEE Robotics and Automation Letters*, vol. 9, no. 2, pp. 1524–1531, 2023.

[10] X. T. Ha, D. Wu, M. Ourak, G. Borghesan, J. Dankelman, A. Menciassi, and E. Vander Poorten, "Shape sensing of flexible robots based on deep learning," *IEEE Transactions on Robotics*, vol. 39, no. 2, pp. 1580–1593, 2022.

[11] S. A. Menaker, S. S. Shah, B. M. Snelling, S. Sur, R. M. Starke, and E. C. Peterson, "Current applications and future perspectives of robotics in cerebrovascular and endovascular neurosurgery," *Journal of neurointerventional surgery*, vol. 10, no. 1, pp. 78–82, 2018.

[12] J. M. Croom, D. C. Rucker, J. M. Romano, and R. J. Webster, "Visual sensing of continuum robot shape using self-organizing maps," in *2010 IEEE International Conference on Robotics and Automation*. IEEE, 2010, pp. 4591–4596.

[13] S. C. Ryu and P. E. Dupont, "Fbg-based shape sensing tubes for continuum robots," in *2014 IEEE International Conference on Robotics and Automation (ICRA)*. IEEE, 2014, pp. 3531–3537.

[14] R. A. Bilodeau, E. L. White, and R. K. Kramer, "Monolithic fabrication of sensors and actuators in a soft robotic gripper," in *2015 IEEE/RSJ international conference on intelligent robots and systems (IROS)*. IEEE, 2015, pp. 2324–2329.

[15] D. Hu, F. Giorgio-Serchi, S. Zhang, and Y. Yang, "Stretchable e-skin and transformer enable high-resolution morphological reconstruction for soft robots," *nature machine intelligence*, vol. 5, no. 3, pp. 261–272, 2023.

[16] P. Xiang, D. Sun, G. Ma, H. Zhang, R. Xiong, Y. Wang, H. Lu, and T. Xu, "A portable and flexible intermediary patch for in vivo magnetic localization," *Nature Sensors*, pp. 1–13, 2026.

[17] J. Wang, Y. Lu, C. Zhang, S. Song, and M. Q.-H. Meng, "Pilot study on shape sensing for continuum tubular robot with multi-magnet tracking algorithm," in *2017 IEEE International conference on robotics and biomimetics (ROBIO)*. IEEE, 2017, pp. 1165–1170.

[18] H. Guo, F. Ju, Y. Cao, F. Qi, D. Bai, Y. Wang, and B. Chen, "Continuum robot shape estimation using permanent magnets and magnetic sensors," *Sensors and Actuators A: Physical*, vol. 285, pp. 519–530, 2019.

[19] G. Pittiglio, A. Donder, and P. E. Dupont, "Continuum robot shape estimation using magnetic ball chains," in *2024 IEEE/RSJ International Conference on Intelligent Robots and Systems (IROS)*. IEEE, 2024, pp. 11 004–11 009.

[20] J. J. Abbott, E. Diller, and A. J. Petruska, "Magnetic methods in robotics," *Annual Review of Control, Robotics, and Autonomous Systems*, vol. 3, no. 1, pp. 57–90, 2020.

[21] T. D. Barfoot, *State estimation for robotics*. Cambridge University Press, 2024.